
ELSEVIER
Remote Sensing of Environment
http://www.elsevier.com/locate/rse

Remote Sensing of Environment 136 (2013) 301–314

Contents lists available at SciVerse ScienceDirect

Remote Sensing of Environment

journal homepage: www.elsevier.com/locate/rse

Integrating terrestrial and airborne lidar to calibrate a 3D canopy model of effective leaf area index

Chris Hopkinson [a,e,*], Jenny Lovell [b], Laura Chasmer [c], David Jupp [a], Natascha Kljun [d], Eva van Gorsel [a]

[a] CSIRO Marine and Atmospheric Research, Pye Laboratory, Clunies Ross St, Canberra, ACT, Australia
[b] CSIRO Marine and Atmospheric Research, GPO Box 1538, Hobart 7001, Tas, Australia
[c] Department of Geography, Wilfrid Laurier University, Waterloo, Ontario, Canada
[d] Department of Geography, College of Science, Swansea University, UK
[e] Department of Geography, University of Lethbridge, Lethbridge, Alberta, Canada

ARTICLE INFO

Article history:
Received 8 January 2013
Received in revised form 9 May 2013
Accepted 9 May 2013
Available online xxxx

Keywords:
Lidar
Leaf area index
LAI
Canopy structure
Airborne/terrestrial laser scanning
Echidna
Point cloud
Percentile distribution

ABSTRACT

Terrestrial laser scanning (TLS) with the Echidna Validation Instrument (EVI) provides an effective and accurate method for calibrating multiple-return airborne laser scanning (ALS) point cloud distributions to map effective leaf area index (LAIe) and foliage profile within a 1-km diameter test site of mature eucalyptus forest at the Tumbarumba research site, New South Wales, Australia. Plot-based TLS foliage profiles are used as training datasets for the derivation of a scaling function applied to calibrate effective leaf area index (LAIe) from a coincident ALS point cloud. The results of this study show that: a) the mean proportion of the total number of returns within 11.3 m radius of the TLS scan station was 64%. Increasing the radius decreased the level of detail due to occlusion; b) the relationship between TLS LAIe profile and ALS foliage percentile distribution (PD) using all, primary and secondary returns are not linearly related; and c) regressions between TLS LAIe profile and ALS PD, demonstrate better correspondence using a 5th order polynomial applied to all returns ($r^2 = 0.95$; SE $= 0.09$ m^2 m^{-2}) than aquasi-physically-based Weibull scaling function. The calibration routine was applied to ALS data within a GIS environment to create a 500 m radius 3D map of LAIe. This localised 3D calibration of LAIe was then used as the basis to calculate the overhead canopy extinction coefficient parameter (k), and thereby facilitate upscaling of spatial LAIe estimates to larger domains using a Beer Lambert Law assumption.

1. Introduction

1.1. Leaf area index (LAI)

The spatial distribution of foliage within a forest canopy controls light and energy transfer between the sky and the ground (Chen et al., 1999; Loranty et al., 2010; Oke, 1996; Traver et al., 2010), the interception of precipitation (Whitehead & Kelliher, 1991; Wilson et al., 2001) and aerosols (Wedding et al., 1975), rates and magnitudes of photosynthesis (Amthor et al., 1990; Chasmer et al., 2008) and evapotranspiration (Blanken et al., 1997; Brümmer et al., 2012; Engel et al., 2002; Ge et al., 2011), atmospheric flux footprint density and extent (Kljun et al., 2002, 2004; McAneney et al., 1994), as well as animal habitat and foraging pathways (DeWalt et al., 2003; Goetz et al., 2010). Consequently, parameters describing leaf properties and canopy structure are necessary inputs to eco-physical models used to simulate mass and energy fluxes throughout forest environments (Davi et al., 2006; Kobayashi et al., 2012; Kowalczyk et al., 2006; Richardson et al., 2012). Recent comparisons between land surface model (LSM) results and observed CO_2 flux (net ecosystem exchange, NEE) at a range of FluxNet sites indicate that models often misrepresent the variability of CO_2 fluxes over short time scales (Schwalm et al., 2010). Phenological processes frequently related to C exchange are most often estimated from remote sensing methods. This has been identified as an area where improvements are needed in model input data (Richardson et al., 2012), and because phenology is inherently related to the amount of photosynthesizing biomass, this requires accurate estimates of leaf area.

Leaf area index (LAI) is typically defined as the vertically integrated one sided area of leaf or needle cover per unit ground surface area on a horizontal plane (e.g. Chen et al., 2006; Gower et al., 1999; Watson, 1947). LAI is expressed in units of m^2 m^{-2} and is traditionally measured through destructive sampling. LAI cannot easily be measured directly through non-destructive means, so another metric, effective leaf area index (LAIe), is more commonly measured in the field and either calibrated to true LAI (e.g. Chen et al., 2006) or used directly in model simulations (e.g. Ives et al., 2011, who use LAIe; and Coops et al., 2012; Schwalm et al., 2010 who use LAI). LAIe is analogous to LAI but does not differentiate between woody or leafy foliage components or account for variations in apparent leaf area due to leaf, branch and shoot

* Corresponding author at: Department of Geography, University of Lethbridge, Lethbridge, Alberta, Canada. Tel.:+1 902 840 1164.
E-mail address: c.hopkinson@uleth.ca (C. Hopkinson).

0034-4257/$ – see front matter © 2013 Elsevier Inc. All rights reserved.
http://dx.doi.org/10.1016/j.rse.2013.05.012

clumping (Chen et al., 1996, 2006; Ives et al., 2011; Ryu et al., 2012). Both methods of characterising foliage distribution are valuable for different reasons, and depend on whether we are interested in leaf surface processes like photosynthesis, respiration and evapotranspiration (Et), or more structural attributes that control energy and mass transfers within the canopy. Therefore, mapping the 3D distribution of canopy LAIe provides a mechanism for modelling and scaling of mass and energy exchanges. The following study compares the 3D distribution of foliage measured using airborne and terrestrial laser scanners at a FluxNet flux monitoring site within a mature mountain ash (*Eucalyptus delegatensis*) forest site in Australia.

1.2. Lidar-based canopy foliage profiles

Airborne laser scanner (ALS) systems employ light detection and ranging (lidar), optical scanner, inertial reference and global positioning system technologies to calculate 3D coordinates of terrain and overlying surface cover (Baltsavias, 1999). ALS surveys are typically optimised for an approximately even spatial sampling of point coordinates. The exact spatial configuration of return sampling patterns varies with scan angle and ALS scanning mechanism (Wehr & Lohr, 1999). There is wide variation in ALS specifications in terms of laser pulse wavelength, power, dimension, repetition frequency and real-time data storage capabilities. In common, however, all ALS data can be outputted as a point cloud of laser pulse returns, with all modern systems able to deliver multiple returns representing the first (uppermost), intermediate and last (lowest) surfaces encountered by each emitted pulse.

LAI (or LAIe) has, in previous studies, been linked to vertical laser pulse return profiles measured using ALS techniques. One simple approach has been to calculate the ratio of the number of returns below the canopy to the total number of returns and assume that this provides a direct estimate of the overhead transmittance or gap fraction (P) of the canopy (e.g. Morsdorf et al., 2006; Riaño et al., 2004; Solberg et al., 2006).

$$P \approx \frac{N_{BC}}{N_{Tot}} \tag{1}$$

where N_{Tot} is the total number of returns in the full canopy profile and N_{BC} is the number of returns below some threshold height above the ground surface (typically between 1 m and 3 m).

It has been shown that while P correlates well with gap fraction and fractional cover, it does not always provide a direct estimate (Hopkinson & Chasmer, 2009). Nonetheless, pulse return ratio techniques can be used to estimate LAIe using an adaptation of the Beer Lambert Law that considers the canopy a turbid medium:

$$LAIe = \frac{-\ln(P)}{k} \tag{2}$$

where k is the extinction coefficient or (in the overhead case) the fraction of total one-sided leaf area projected onto a horizontal plane. For simplicity, k is often assigned a value of 0.5 following an assumption of random or spherical leaf distribution (Martens et al., 1993). In practice, overhead k values are highly variable in forest canopies, ranging approximately between 0.25 and 0.75 (Jarvis & Leverenz, 1983). Higher values indicate more planophile (horizontal) leaf orientations, while lower values indicate more erectophile (vertical) orientations.

Magnussen and Boudewyn (1998) found that the cumulative percentile distribution (PD) of ALS return heights collected at a resolution of ~1 pt per 5 m^2 showed no significant difference with plot-level models of cumulative needle leaf area distribution for several Douglas-fir plots. This observation of no significant difference between foliage and ALS profiles has tended to be corroborated in more recent studies where data densities have been closer to 1 pt m^{-2}. (e.g. Coops et al., 2007; Todd et al., 2003) and also ALS distributions recreated using intensity (an analogue for signal return strength) and not just the return frequency (e.g. Lovell et al., 2003). While these observations hold within the level of confidence possible within each study, it needs to be considered that the PD is sensitive to some aspects of sensor configuration such as scan angle (Holmgren et al., 2003), pulse power (Chasmer et al., 2006), beam divergence and altitude (Hopkinson, 2007; Næsset, 2009). Consequently, as measurement accuracy, data resolution and model requirements increase, we need to adapt our understanding of ALS characterization of foliage profiles and make adjustments to the way we estimate ALS-based canopy properties.

Due to higher repetition rates and multiple return capture, modern ALS sensors can generate laser pulse return densities at least two to three orders of magnitude greater than early generation sensors. Consequently, the point clouds associated with newer technologies provide increasingly greater detail of tree stem, branch and canopy architecture (e.g. Adams et al., 2012; Allouis et al., 2012; Lindberg et al., 2012; Reitberger et al., 2009) as opposed to the more low density sampling of horizontal canopy foliage layers achieved with earlier generations of sensor technology. This high data density is valuable from the perspective of visualising canopy architectural detail but it means that the point cloud and associated PD are likely to represent more than just the leaf or needle area. This is particularly the case with wider scan angles, where more vertical elements within the canopy will be captured (Holmgren et al., 2003). As a result, modern ALS data captured over forested areas are starting to approach similar levels of structural information as terrestrial laser scanner (TLS) point clouds (Fig. 1), where dense datasets characterising stem-level attributes have been the norm for almost a decade (Côte et al., 2011; Hopkinson et al., 2004; Lovell et al., 2003). This poses a challenge, as it means that earlier assumptions about relating that the ALS point return PD to the canopy leaf area profile may not be applicable to high density, wide scan angle ALS data that is increasing in popularity and availability.

The simplest way to address this challenge is to apply an empirical calibration to the ALS PD that is trained by field-based measurements of the foliage profile. If, as suggested by early studies, the ALS PD generated from modern high-density wide-scan point cloud data matches the field-based foliage profile, then a histogram-matching calibration process should result in a simple linear scale factor to relate the two profiles. If the two profiles are not linearly related, then a non-linear scaling function that varies with profile height (z) will be necessary. A reliable field-based method of canopy foliage profile generation using the Echidna® Validation Instrument (EVI) TLS system has been demonstrated in a number of studies (Jupp et al., 2005, 2009; Lovell et al., 2003, 2011; Strahler et al., 2008). The approach presented here is to use plot-based EVI foliage profile data as training datasets to generate a histogram scaling function, which can be used to calibrate a profile of LAIe from the vertical PD of a coincident ALS point cloud. This calibration is then applied to ALS data captured at a FluxNet monitoring site in Australia to generate a 3D model of canopy foliage distribution within the footprint of the flux monitoring tower.

1.3. The Echidna® Validation Instrument (EVI)

The EVI (Jupp et al., 2009; Lovell et al., 2003; Strahler et al., 2008) is a waveform-recording, multi-view angle TLS system. It is designed to capture data from at least the full upper hemisphere in a single acquisition and cover the field of view with no gaps in laser illumination (Jupp et al., 2005). The scanning pattern of the EVI is controlled by a rotating mirror that directs the beam through the vertical plane, and by rotation of the sensor head to provide azimuthal coverage. The rotation rate is normally selected to provide contiguous shots at the horizontal and overlapping data closer to zenith. The optical system is coaxial, which provides an efficient optical system, compact assembly and essentially no minimum detectable range. The optical design of the instrument means that some of the outgoing laser pulse is present in the recorded signal, which allows precise temporal alignment of the individual waveforms.

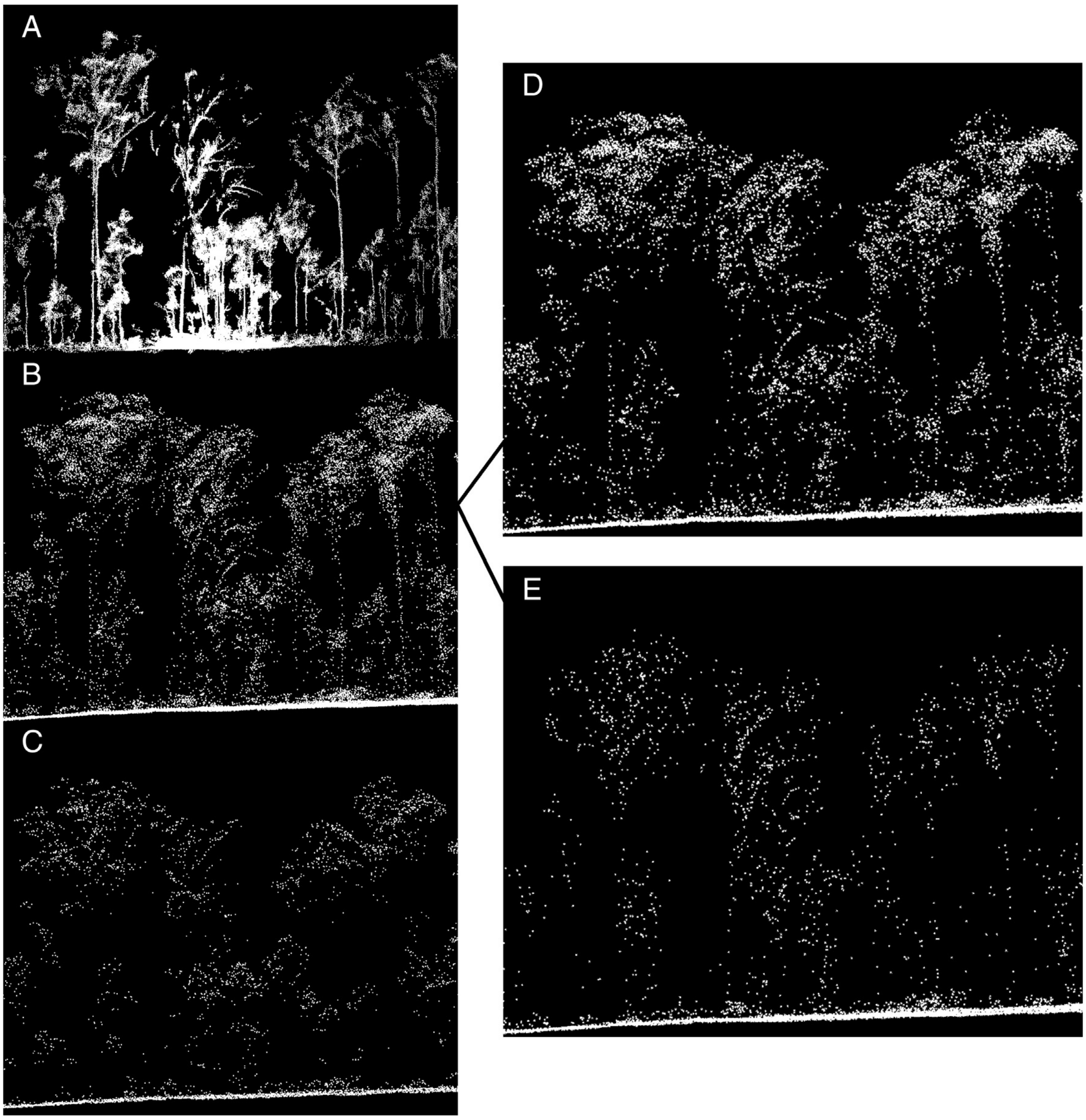

Fig. 1. A 5 m deep and 50 m wide cross section through three independent laser pulse return point clouds at the centre of a mature *Eucalyptus delegatensis* EVI plot at Tumbarumba. A) EVI TLS data captured using the EVI from ground level looking up; B) all return high resolution (~26 pts/m^2) wide scan (±30°) ALS data illustrating vertical stem and some branching structure; C) all return medium resolution and scan angle ALS data (~5 pts/m^2 and ±20°) with no obvious signs of stem representation; D) primary returns from 'B' (17 pts/m^2); E) secondary returns from 'B' (9 pts/m^2). All data captured near midsummer and within one year apart.

The EVI uses a diode pumped solid state 1064 nm Nd:YAG laser operating at a fixed pulse repetition frequency of 2 kHz. The outgoing beam has a diameter of 29 mm with a manually variable divergence of between 2 and 15 mrad. Empirical tests of temporal pulse shape have determined that the pulse width has a stable value of 14.9 ns at full-width half-maximum which corresponds to an effective width in 'range' of about 2.4 m. Despite the width of the pulse the peak is sharp and well defined, allowing accurate determination of range to targets producing a single clear return.

In contrast to many TLS systems that record a single range for each laser shot, the EVI records the light reflected from objects along the laser path which can be calibrated to power units. The waveform is recorded with a maximum sampling rate of 2 GS s^{-1} which equates to one sample every 7.5 cm of range from the instrument. In addition to the core waveform data, ancillary information is recorded continually throughout a scan. The data recorded have three geometric dimensions; zenith angle ($0 \leq \theta \leq 180°$), azimuth angle ($0 \leq \varphi \leq 360°$) and range (r) to target. The precise positional information that is recorded allows the data to be projected into a number of different formats. The known laser pulse shape allows filtering of the waveform data to produce point clouds (Yang et al., 2013) of detected target locations.

2. Study area

The Tumbarumba study site is in the Bago State Forest of the southern tablelands of New South Wales, Australia. It has a moist temperate climate with annual precipitation ~1500 mm and a mean annual temperature of 8.0 °C (Leuning et al., 2005). The wet sclerophyll forest site lies between 1200 and 1300 m a.s.l., is dominated by mature alpine ash (*E. delegatensis*) with stem heights up to 50 m (Fig. 2) and is an area of active forest management. A flux monitoring tower was installed in 2000 at the boundary of two stands that were commercially thinned in 1984 and 1985. Surrounding forest stands (>500 m from the tower) have undergone periodic commercial thinning operations. Annual net carbon exchange within the footprint of the tower is highly variable but over the long term the site has been found to be a net carbon sink (van Gorsel et al., in press).

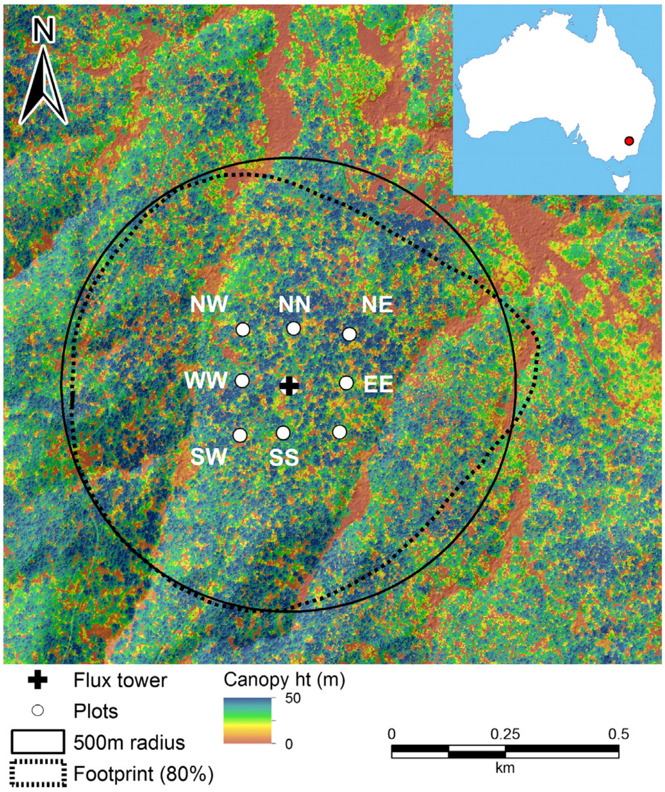

Fig. 2. The Tumbarumba forest study site, illustrating canopy height, eddy covariance flux tower and TLS plot locations (and names for the seven used in model development), 80% flux footprint extent and 500 m radius surrounding the tower. Inset is the site location within Australia.

For the purpose of this analysis, the 3D LAIe mapping area of interest (AOI) was limited to a 500 m radius of relatively homogenous and recently undisturbed canopy surrounding the tower (Fig. 2). This area corresponds closely to the 80% flux footprint probability density function associated with long term flux measurements from 2001 to 2011 (Hopkinson et al., 2012; van Gorsel et al., in press). From the flux footprint parameterization of Kljun et al. (2004), ~50% of the long term flux originates from within 200 m of the tower but this drops off quickly with 86% being contained within the 500 m radius AOI and 91% for a radius of 1 km. The radius derived from the footprint parameterization is relatively short due to the high surface roughness and the prevailing stability conditions found at this site. Consequently, while the AOI extends out to 500 m, our requirement for model accuracy increases closer to the tower where canopy conditions have a more direct influence on measured and modelled CO_2 and H_2O fluxes.

3. Data

Summertime ALS data were captured in November 2009 using a Riegl LMS-Q560 operating at a wavelength of 1550 nm, a beam divergence of 0.5 mrad and using a rotating polygonal mirror to distribute laser pulses across a linear swath beneath the survey aircraft. The sensor was flown at approximately 400 m a.g.l with a $\pm 30°$ maximum scan angle, 240 kHz pulse repetition frequency and 50% swath side lap to ensure that all areas were viewed from two positions. For each pulse emitted, the full waveform return was recorded and then converted to multiple discrete returns in post-processing. The derived point cloud had a mean scan angle at ground level of ~15° and a horizontal multiple return point density in the AOI of ~26 pts m^{-2}(Fig. 1B). TLS data were captured with the EVI two times at eight plots in the area of maximum flux origin on a grid of 300 m × 300 m immediately surrounding the flux tower (Figs. 1A and 2). In all cases beam divergence was set to 5 mrad. One sample set was collected in February 2009 (nine months prior to the ALS) and another in December, less than one month following the ALS. The December TLS was used for ALS LAIe profile calibration due to temporal proximity. To facilitate georegistration of the TLS and ALS point clouds, the EVI scanner locations were surveyed using single frequency rapid static differential GPS to within ~1 m absolute accuracy in December of 2009. Digital hemispherical photographs (DHPs) were captured at the eight TLS plots in February 2009 to provide some local validation of the TLS-based total LAIe estimates. Canopy LAIe was calculated from the DHPs using the LAI_{57} approach in the CAN-EYE software (Weiss & Baret, 2010). This approach was chosen, as we have no reliable data describing clumping or leaf angle distribution, and LAI_{57} isolates the hemispheric gap fraction at 57.5° where a random foliage distribution can be reasonably assumed (Warren-Wilson, 1963; Weiss et al., 2004).

4. Methods

4.1. EVI $LAIe_{TLS}$ profiles

Profiles of foliage area are related to the vertically resolved gap probability distribution within the canopy, P_{gap}.

$$P_{gap}(\theta, z) = e^{-G(\theta)L(z)/\cos\theta} \tag{3}$$

where θ is the zenith angle, z is the height above ground, $G(\theta)$ is the Ross G-function (Ross, 1981) and $L(z)$ is the cumulative (or total) foliage area at height z. An estimate of $P_{gap}(\theta,z)$ can be obtained from the EVI data as presented below. Thus the profile of LAIe can be calculated and its derivative, the foliage area volume density.

The calculation of P_{gap} from EVI data follows the method of Jupp et al. (2009). All the EVI waveforms are captured from a hemispherical scan and individually processed to a quantity called apparent reflectance. This is the reflectance of a diffuse target filling the beam of the instrument that would return the same intensity as recorded from the actual target. For a waveform recorded at zenith angle, θ, over ranges, r, it has the form

$$\rho_a = \frac{I(\theta, r)R^2}{K(R)\Phi_0} \tag{4}$$

where I is the range-dependent recorded intensity, R is the range to the target, $K(R)$ is a calibration function associated with the geometry of the receiver optics and Φ_0 is the energy of the outgoing pulse. Integrating ρ_a over range provides a step-wise reduction in the power of the outgoing signal brought about by hits on single or multiple targets. This is related to P_{gap} by

$$I_a(\theta, r) = 1 - p(\theta, g)\left(1 - P_{gap}(\theta, r)\right) \tag{5}$$

where I_a is the integral of ρ_a, g is the distribution function for facet directions of the targets and p is the mean phase function for the varying facets. In general, the phase function is unknown and if possible should be estimated from the data. Jupp et al. (2009) use an initial assumption of $p = 1$ and then identify two thresholds in the calculated P_{gap} relating to (i) the maximum P_{gap} value for targets that fully extinguish the beam (hard target) and (ii) the maximum P_{gap} value for targets that partially extinguish it (soft target), above which all samples are assumed to be true gaps. These are used to scale the P_{gap} in a similar way to the two-level separation of gap and vegetation that can be done in hemispherical photograph analysis (Leblanc et al., 2005).

The value of P_{gap} calculated from a single waveform is a realisation of an actual gap, rather than a probability, therefore it is necessary to average the measured values over some spatial region in order to estimate the underlying probability distribution. In this work, the EVI data are averaged over rings between zenith angle limits in steps of 5°. We calculate a mean foliage profile from zenith-ring averages of P_{gap} using the ratio of cumulative foliage area ($L(z)$) relative to LAIe to provide a profile largely independent of clumping. The effect of clumping is subsumed into the empirical Ross-G function that is part of the linear LAIe model (Jupp et al., 2009). Thus the cumulative LAIe profile (or total LAIe) is defined by

$$\frac{L(Z)}{LAIe_{TLS}} = \frac{\ln P_{gap}(\overline{\theta}, z)}{\ln P_{gap}(\overline{\theta}, H)} \tag{6}$$

where H is the height of the canopy and the notation $\overline{\theta}$ indicates that the data are averaged over a range of zenith angles, rather than a mean angle. The foliage area volume density profile is then

$$f(z) = LAIe_{TLS} \frac{\partial}{\partial z}\left(\frac{\ln P_{gap}(\overline{\theta}, z)}{\ln P_{gap}(\overline{\theta}, H)}\right). \tag{7}$$

In these equations the value of $LAIe_{TLS}$ is estimated from the EVI data using a simple linear canopy model as shown by Jupp et al. (2009). The P_{gap} profiles are calculated for a number of zenith rings i.e. different values of $\overline{\theta}$, and then a mean profile is calculated by weighting each profile according to the solid angle subtended by the ring.

4.2. Data alignment and plot extraction

Combining ALS data captured from an overhead moving platform with static hemispheric TLS data captured from a point on the ground presents two primary challenges: i) the point clouds must be horizontally and vertically co-registered to ensure that 3D attributes are directly comparable; ii) sampling geometry and laser pulse occlusion mean that the horizontal and vertical distributions of point cloud density are not equal. Addressing the first challenge was straight forward as each EVI scan location had been surveyed, such that the origin of the scanner could be set to the known GPS coordinate. Orientation and fine horizontal and vertical adjustments of the TLS point cloud were achieved by translating and rotating the TLS data until they visually matched the ALS data. Automated least squares approaches are available for scan alignments using off the shelf commercial software but this approach can be problematic and lead to erroneous results using TLS data in complex forested environments (e.g. Hopkinson et al., 2004), so a manual interpretive approach was preferred.

The irregularity of point cloud sample distributions between ALS and TLS has both vertical and horizontal elements. The vertical differences in sampling density and frequency distributions are the subject of the LAIe histogram-matching calibration (described below). However, the horizontal sampling density variation must be addressed in the selection of a suitable plot size for subsequent calibration of the ALS data. Spatial sample density for ALS data can be assumed to be relatively even, whereas TLS data density will systematically diminish with distance from the scanner (Fig. 1A) due to increased point spacing and foliage-induced occlusions (Chasmer et al., 2006; Côte et al., 2012). A similar challenge must be addressed when matching DHP estimates of LAI or fractional cover with ALS data at the plot-scale (Hopkinson & Chasmer, 2009; Morsdorf et al., 2006).

Given the systematic decrease in TLS sample density and increasing randomness in TLS sample coverage at ever larger radii, a suitable ALS sampling radius around the EVI scanner was identified by measuring the proportions of the total TLS sample points present within four different radii for each of the EVI plots. It is a priori understood that the radius cannot be too small as to contain too few of the foliage contact points used in the LAIe profile generation, while it cannot be too large as to lose its spatial representivity or uniqueness. The radii tested followed an approximately logarithmic pattern of increasing area 11.3 m (0.04 ha) to 25 m (0.2 ha) to 56 m (1 ha) to 100 m (3 ha). The smallest radius corresponds to a forest mensuration plot of 400 m^2, which is small enough to contain unique tree crown attributes from a single or small number of Eucalyptus trees while being large enough to ensure mis-alignments and spatial uncertainties are mitigated. The largest radius corresponds to the approximate distance between EVI plot centre locations, and results in up to 40% areal overlap between plots; i.e. beyond this radius, the plots will possess spatial auto correlation and cannot be used as independent training data points. The 56 m radius approximates the midpoint between plots where there is no appreciable overlap and is also close to the distance at which a 57.5° zenith angle from the EVI scan location emerges from the canopy of the Eucalyptus stand; i.e. the angle at which foliage orientation can be assumed to be random (Warren-Wilson, 1963; Weiss et al., 2004). The 25 m radius is logarithmically approximately mid way between 11.3 m and 56 m. Once a suitable radius was identified, ALS point cloud data surrounding each of the EVI plot centres were extracted for comparison and calibration.

4.3. ALS profile calibration

Ground-level TLS data captured below the horizontal plane of the EVI scan origin were not used in the generation of the $LAIe_{TLS}$ profile. Therefore, during the histogram-matching calibration process, only ALS data lying above the height of the EVI scanner origin were used. This height varied between 1.6 m and 1.9 m above ground. ALS data above this plane at each EVI plot were binned at 2 m height increments for subsequent comparison and histogram-matching. Bin heights of 2 m were chosen, as this provided a suitable compromise between the requirements for sufficient detail in the foliage profile while being large enough to accommodate positional and alignment uncertainties that, in extreme cases, could approach 1 m. The ALS data were converted to a percentile distribution (PD) by counting the number of points within the previously determined 'optimal' radius for each 2 m high bin, and then dividing into the total number of points within the profile. The PD could then be directly compared to $LAIe_{TLS}$ on a bin by bin basis. Comparisons were performed on three return classes of ALS data: i) all returns (first, single, intermediate and last echoes) to maximise the sampling density of the ALS data and increase the level of canopy structural detail; ii) primary returns (first and single echoes — Fig. 1D) to be consistent with early ALS foliage profile recreation techniques (e.g. Magnussen & Boudewyn, 1998); and iii) secondary returns (intermediate and last echos — Fig. 1E), as these returns penetrate the outer envelope of the canopy and have the potential to characterize foliage structure that is partially occluded and therefore invisible to primary returns.

Comparison of $LAIe_{TLS}$ profiles with the ALS PD profiles was performed at seven of the eight EVI plot locations surrounding the flux tower. [One EVI scan was omitted from the analysis, as the raw scan data could not be retrieved.] The first test performed was to ascertain which of the all ($PD_{(ALL)}$), primary ($PD_{(P)}$) or secondary returns ($PD_{(S)}$) provided the most robust dataset for calibration of the $LAIe_{ALS}$ model. This test was performed using a polynomial regression histogram-matching technique to force the average of the seven ALSPD profiles to fit the average of the $LAIe_{TLS}$ profiles:

$$LAIe_{(z)} = a_{(z)} PD_{(z)} \tag{8}$$

where a is a scaling factor that varies with bin height z. Polynomial functions of the scale factor a were derived by dividing $LAIe_{TLS}$ by PD for each of the six plots and averaging the results for each of the height bins from 2 m to 50 m (max canopy height) above ground level. The suitability of all, primary or secondary returns for LAIe histogram matching was determined based on the comparative results of the polynomial regressions. The polynomial regression functions ranged from third to sixth order, with the order chosen based on observable improvements in the coefficient of determination; i.e. if the r^2 value continued to increase at each order, then a sixth order polynomial would be chosen for the calibration. Higher orders of polynomial were not considered due to the likelihood of overfitting the data.

Following determination of the optimal point return class for LAIe profile reconstruction, it was decided to test two 'robust' approaches for calibration that could either be 'tweaked' for future datasets and for different areas, or applied over small areas with minimal mathematical manipulation. Polynomial regression was not considered ideal for widespread implementation, as it has no physical basis and can be manipulated to fit almost any curve; even one containing errors. Two approaches were adopted. The first, a quasi-physical approach, was to model *a* as a function of either one or two Weibull distributions (e.g. Coops et al., 2007; Lovell et al., 2003; Magnussen et al., 1999). The implicit assumption here being that the scale factor *a* varies as a function of the foliage density

$$a(z) = q\left[1 - e^{-r\left(1-\frac{z}{h}\right)^{s}}\right] \tag{9}$$

where *q*, *r*, and *s* are the fitted parameters. A single and a double Weibull curve approach were attempted, as the forest at Tumbarumba possesses significant understorey foliage and displays a two tier foliage distribution in some places. For the single Weibull scaling function, Eq. (9) was fitted to the complete canopy height range. In our implementation of a double Weibull curve, the height-based scale factors were separated into two canopy components based on the height of the inflection point between under- and over-storey components. The understorey scaling function was computed first. Then the scale factor residuals between the first iteration of Eq. (9) and the overstorey were used in a second iteration of Eq. (9) to derive a second Weibull scaling function, which, when added to the first, produced a scaling function for the full canopy profile.

The second approach to calibration was the simplest to implement while also being the most accurate in terms of honouring the original calibration data; i.e. to calculate an independent scale factor *a* for each bin height and use a 'look up table' approach. This was the approach applied to the ALS data surrounding the tower at Tumbarumba, as the AOI was small and the calibration data collected from the region of most interest for future modelling.

4.4. $LAIe_{ALS}$ model

Following the histogram-matching calibration process, the model needed to be applied to the elevation- and height-variant canopy ALS point cloud data across the AOI. For simplicity, 2.0 m was chosen as the threshold between canopy and ground level foliage cover. This height is convenient and broadly justified as it is close to that of the EVI scanner origins, approximates that used in the DHP canopy LAIe measurements and is typical for ALS-based canopy to ground height ratio thresholds. Moreover, within a reasonable height range (say 1 m to 3 m) choosing a precise height threshold is somewhat arbitrary, so choosing a height that corresponds exactly with the first height bin above the ground surface simplifies analytical procedures and the presentation of data.

ALS ground points were filtered from single and last return points using an adaptation of the ground classification algorithm developed by Axelsson (1999). All individual ALS point elevations were normalised to height above ground following the approach described in Hopkinson et al. (2006). As with the calibration process, all ALS data were binned into 2 m high increments. The ground-level bin (0 m to 2 m) was needed for the construction of the vertical PD but an estimate of LAIe below the canopy threshold was not possible due the mixture of ground and vegetation points within this height range. The 3D model was implemented by gridding each bin as an independent raster layer and then stacking the layers to generate a spatially varying PD. A grid cell resolution of 2 m was chosen to be consistent with the vertical bin resolution. To ensure that the model calibration was applied over an equivalent spatial domain to that from which it was derived, grid level PD values were calculated using a search radius equivalent to the optimal plot radius established earlier. The scaling functions derived during the calibration process were then applied to each bin layer to generate a vertically stacked map of $LAIe_{ALS}$ at a 2 m × 2 m × 2 m voxel resolution throughout the 500 m radius AOI.

For the sake of comparison and to provide an estimate of site LAIe using methods similar to previous studies, a map of total LAIe was created using the ALS return ratio (Eq. 1) and Beer Lambert Law approach (Eq. 2). An extinction coefficient *k* of 0.5 (spherical foliage distribution) was assigned, as the true value was not known. By comparing the mean LAIe estimates from the two maps surrounding the tower, it was possible to then calculate a more realistic value for *k* (e.g. Morrison et al., 2011).

5. Results and discussion

5.1. EVI vs DHP LAIe

No DHP data were captured at the time of the ALS and TLS collections in late 2009. However, EVI $LAIe_{TLS}$ and DHP $LAIe_{57}$ captured almost 10 months earlier in February 2009 demonstrate comparable results over eight coincident plots surrounding the tower (Fig. 3). A t-test demonstrated that there was no significant difference in mean LAIe estimates using DHP ($1.58\ m^2\ m^{-2}$, $\sigma = 0.20$) or EVI ($1.57\ m^2\ m^{-2}$, $\sigma = 0.23$), and despite a limited range in LAIe observations the relationship between DHP and EVI LAIe was strong ($r^2 = 0.64$) and close to unity (slope = 0.99). These observations are similar to results presented in Lovell et al. (2012) and indicate that the total LAIe estimates derived from EVI around the tower site at Tumbarumba are consistent with more traditional DHP-based methods of LAIe measurement. While the EVI-derived foliage profile is not directly validated, the observed correlation between plot-level EVI and DHP total LAIe supports the assumption that EVI-derived LAIe profiles are a suitable data source for the calibration of ALS LAIe profiles.

5.2. EVI plot radius

For all EVI plots, a mean of 64% of all points was captured within 11.3 m horizontal radius of the scan station (Table 1). Increasing the radius to 25 m raised the mean proportion of data captured from 64% to 82% despite a 500% increase in the area sampled. At 56 m, 95% of all data had been captured but canopy structure detail was sparse due to occlusion caused by dense foliage elements closer to the scanner. Beyond 100 m radius (9 times greater distance and 80 times greater

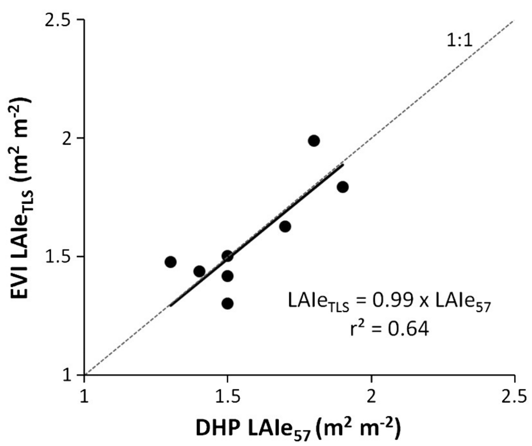

Fig. 3. EVI vs DHP LAIe for the eight plots surrounding the flux tower in February 2009.

Table 1
EVI scan data point totals by radius out from scanner origin.

Radius (Area)	Percentage of total points sampled in the EVI scan							Mean
	EE	NE	NN	NW	WW	SW	SS	
11.3 m (0.04 ha)	74%	57%	57%	64%	66%	67%	59%	64%
25 m (0.2 ha)	90%	82%	81%	82%	84%	80%	78%	82%
56 m (1 ha)	99%	98%	96%	98%	96%	92%	90%	95%

area than at 11.3 m) only occasional points were retrieved at a density too low to be of any value.

Regressing the ALS $PD_{(All)}$ bin values against the comparable EVI LAIe values produced very weak correlations ($r^2 < 0.1$ at all radii) but the smaller 11.3 m radius demonstrated slightly better results (closer to unity and higher r^2) than either 25 m or 56 m. There are compelling reasons for choosing 11.3 m as the plot size for EVI to ALS LAIe calibration: i) EVI data are densest and less sensitive to occlusion closer to the scan station and so the profile is more representative of the foliage profile immediately surrounding the EVI location; ii) terrain and canopy height variations are reduced at smaller radii; iii) 11.3 m radius corresponds to a standard mensuration plot size of 400 m^2 and is equivalent in area to a 20 m × 20 m grid cell, which represents a convenient array size for modelling canopy properties around flux towers. A smaller radius was not practical, as this would mean that the region of extracted ALS data would be much smaller than that containing the TLS data used in the generation of the $LAIe_{TLS}$ profiles.

5.3. The influence of return classification

Comparisons of plot-level $LAIe_{TLS}$ to ALS primary ($PD_{(P)}$) and secondary ($PD_{(S)}$) return class percentile distributions extracted from the 11.3 m radius around the EVI scanner are illustrated in Fig. 4. Due to primary (first and single echo) returns comprising almost 70% of the total point cloud, the shape of $PD_{(All)}$ (not shown in Fig. 4) is virtually indistinguishable from $PD_{(P)}$. In most cases, the ALS and TLS profiles display bimodal distributions describing the upper canopy and understorey. As has been reported elsewhere (e.g. Chasmer et al., 2006) the primary and

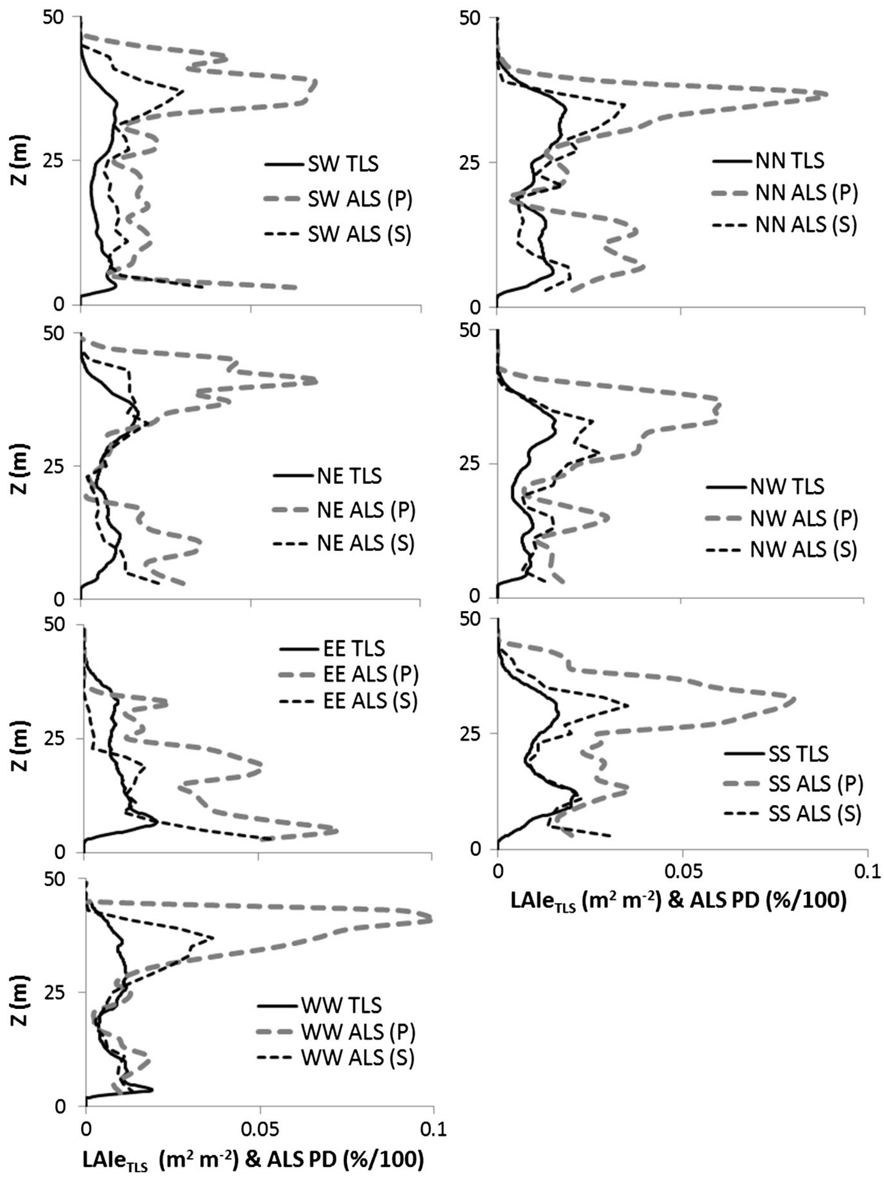

Fig. 4. $LAIe_{TLS}$ profiles with ALS percentile distributions (PD) for primary (P) and secondary (S) returns at seven plots. ALS data binned in 2 m height increments.

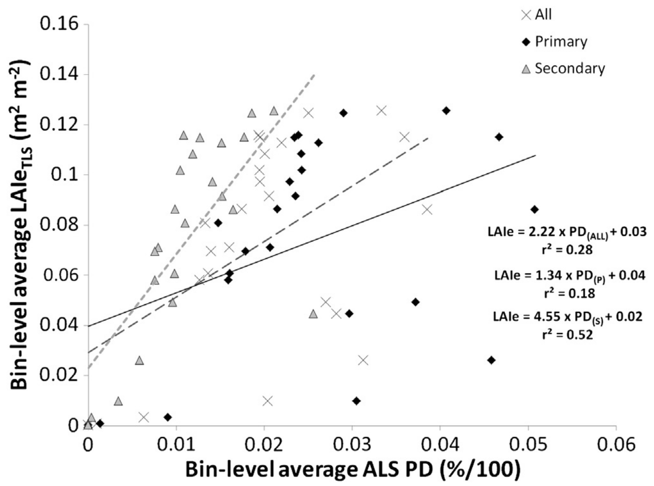

Fig. 5. Height bin-level regression of average $LAIe_{TLS}$ and ALS PD for all returns (ALL), primary returns (P) and secondary returns (S). Using direct linear regression, secondary (last and intermediate) returns demonstrate best fit. (Note: bin height averaged across all seven plots).

all return ALS profiles tend to peak higher in the canopy and characterize less of the understorey than the associated TLS profiles. Visually, it is not easy to identify which of the ALS return class profiles most closely matches the shape of the $LAIe_{TLS}$ profiles but it is clear they are not strongly linearly related (Figs. 4 and 5) with some random variations between coincident profiles. Indeed, from Fig. 5, the most direct correlation between the average ALS and TLS profiles is found for $PD_{(S)}$. While this is not a strong relationship ($r^2 = 0.52$), it is interesting that the lower density secondary returns comprising less than 10% of the canopy-level point cloud (>20% is below the canopy height threshold of 2 m) provide a more direct index of the foliage distribution than the more dense primary returns.

The minor improvement in r^2 from 0.18 to 0.28 from $PD_{(P)}$ to $PD_{(ALL)}$ in Fig. 5 is due to inclusion of secondary returns. None of the linear regression models presented in Fig. 5 provide a useful basis for simulating LAIe from the ALS PD, as it is clear from Fig. 4 that scaling between $LAIe_{TLS}$ and ALS PD varies with height (z). This is better illustrated in Fig. 6, where the scaling function a is derived through polynomial regression and applied to the average $PD_{(ALL)}$, $PD_{(P)}$, and $PD_{(S)}$ for all seven plots. While secondary returns provide the most direct correlation with height bin-level $LAIe_{TLS}$ (Fig. 5), the height-dependent scaling function is more

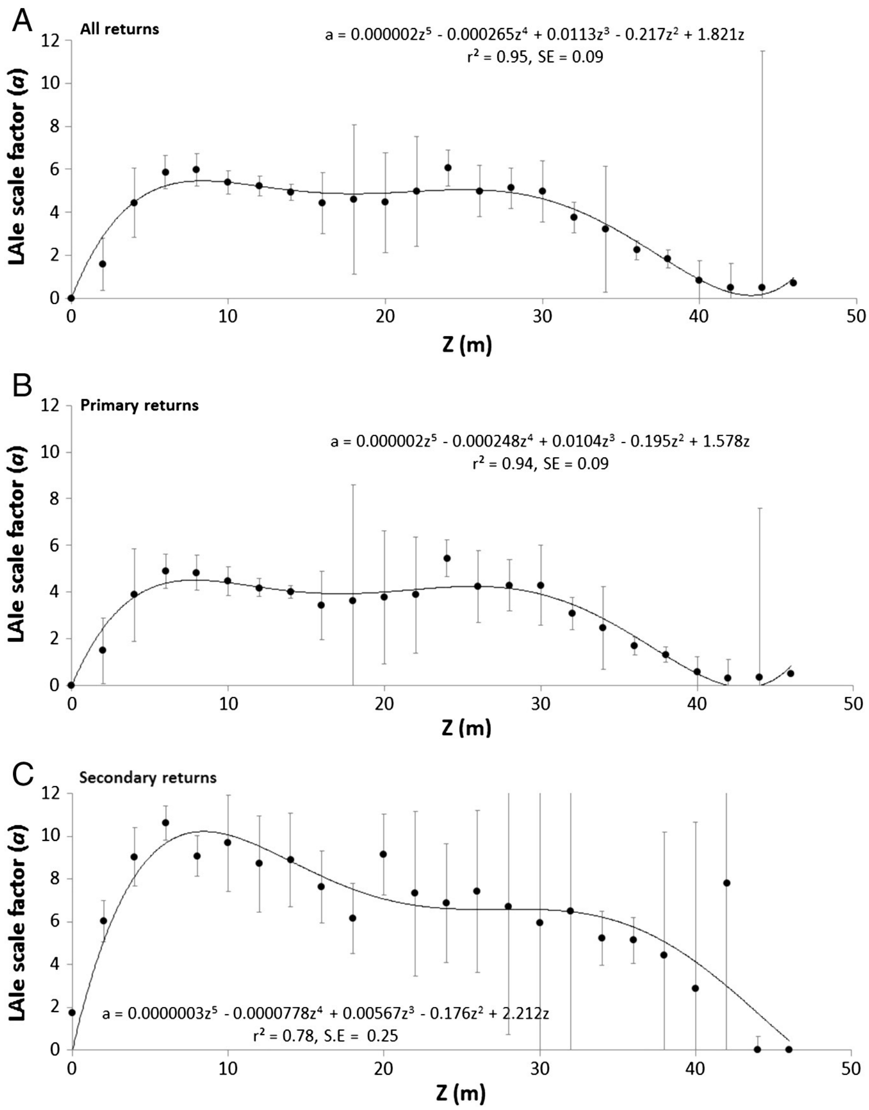

Fig. 6. 5th order polynomial scaling functions a to match the ALS PD of all (A), primary (B) and secondary (C) returns to the EVI $LAIe_{TLS}$ profile. Error bars = one standard deviation of the bin height scale factor across all seven plots. Note: $z = 0$ in this figure is the scanning plane origin.

uniformly distributed and predictable for all and primary returns (Fig. 6). A 5th order polynomial regression of the mean scaling function *a* with respect to height *z* (Fig. 6) demonstrates that $PD_{(ALL)}$and $PD_{(P)}$can be more easily matched to the EVI LAIe profile ($r^2 = 0.95$, 0.94and SE = 0.09, 0.09, respectively) than when using ALS $PD_{(S)}$(r^2 = 0.78, SE = 0.25). Given that $PD_{(ALL)}$ results in a slightly better model fit and contains higher density point sampling throughout the canopy profile, it is considered the most suitable of the three return class distributions tested for matching with the EVI-derived LAIe distribution.

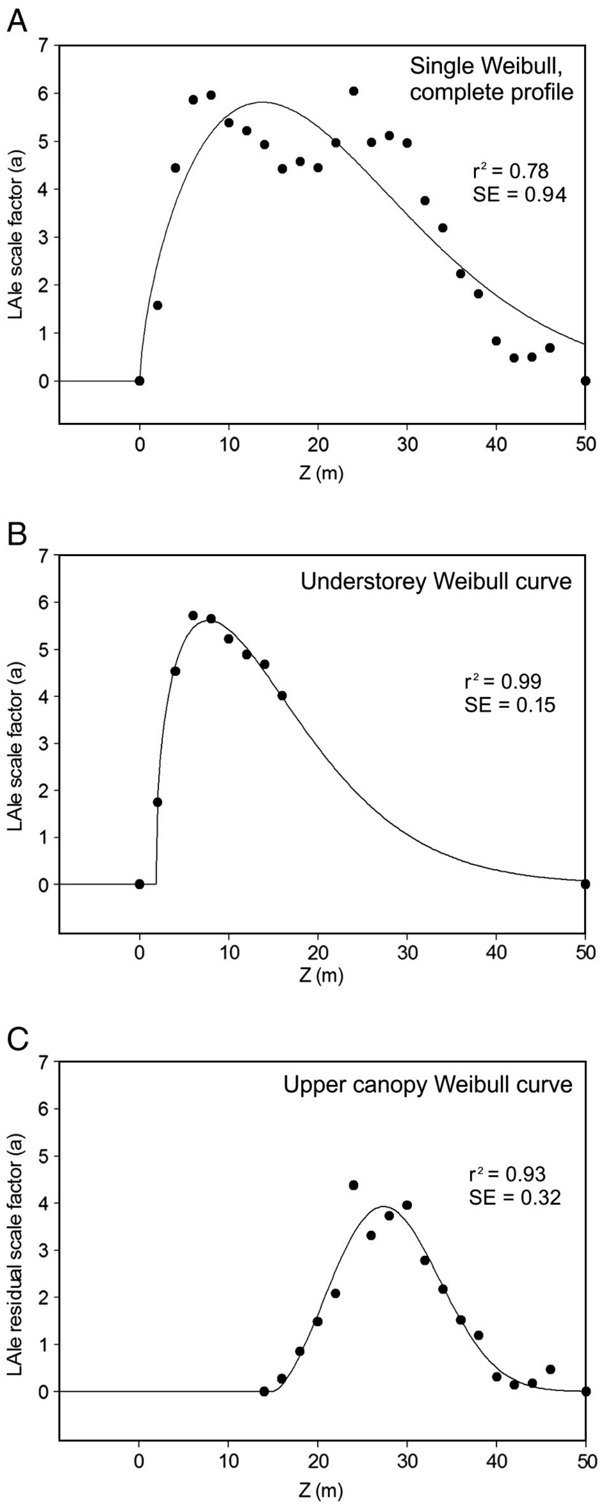

Fig. 7. Weibull curves fitted to the ALS $PD_{(ALL)}$ scale factor *a* distribution with height *z* for: A) the complete canopy profile; B) the understorey profile; and C) the upper canopy residuals after fitting the understorey curve.

5.4. Weibull curve scale factor

After selecting ALS $PD_{(ALL)}$ for all subsequent analysis, the Weibull-based scaling function results (Fig. 7) demonstrated no improvement over those of the polynomial curve fitting approach. It is clear that a single Weibull distribution (when fitted from the ground up) is inadequate to fit the entire scaling function ($r^2 = 0.78$, SE = 0.94 $m^2\ m^{-2}$), as it does not capture the two-tier canopy (Fig. 7A). Splitting the scaling function data into two independent curves, however, improves the fitting capability of the Weibull distributions, with the understorey (Fig. 7B) and upper canopy (Fig. 7C) curves demonstrating high r^2 values of 0.99 and 0.93, respectively. While these r^2 values are comparable to the 0.95 value achieved by the 5th order polynomial in Fig. 6, the standard error of estimate (SE) statistics is weaker. The SE values of 0.15 $m^2\ m^{-2}$and 0.32 $m^2\ m^{-2}$for the understorey and upper canopy curves, respectively, are both high compared to that of the single 5th order polynomial of 0.09 $m^2\ m^{-2}$. Even when the two Weibull curves are combined and the standard error recalculated, the combined value becomes 0.21 $m^2\ m^{-2}$, which is still high compared to the polynomial approach.

The poor performance of the single and double Weibull curve scaling functions relative to the polynomial regression method was not surprising given that the Weibull distribution is constrained to a particular shape that can be considered similar to a skewed Gaussian distribution. Conversely, a 5th order polynomial curve has substantial freedom in terms of its shape and relative ‘peakiness’ or ‘flatness’ along the distribution. Nonetheless, the value in the Weibull distribution approach is that the curves have a similar characteristic to the scaling function elements associated with each of the two tiers in the canopy. It appears from Figs. 6 and 7 that the average scaling function varies with height along the foliage profile, such that scale factor increases near the base of the

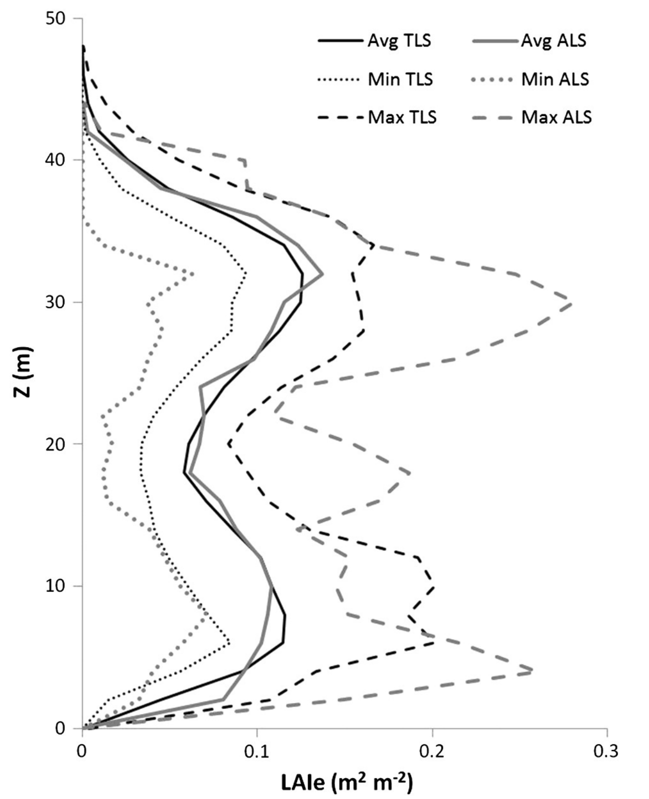

Fig. 8. TLS and Histogram-matched calibrated all returns ALS LAIe profiles for seven plots around the flux tower. Profile values illustrate the min, max and avg of all seven values across all scan locations at the indicated height.

upper and lower tiers in the canopy, decreasing towards the outer or upper edge of the canopy where foliage is well represented in the ALS point cloud. Consequently, the assumed physical basis for adopting a Weibull curve scaling function may be well-founded and likely to produce 'realistic' results, in situations where training data are sparse or not spatially representative of all areas to be mapped.

5.5. ALS LAIe model implementation

The histogram-matched bin-level lookup table scaling function values are presented in Fig. 8. The average EVI $LAIe_{TLS}$ profile matches the calibrated $LAIe_{ALS}$ with a similar range in the maximum and minimum LAIe bin-height values across all seven plots around the flux tower. The standard error for the calibrated plot-level mean foliage profiles was 0.01 $m^2\ m^{-2}$, thus demonstrating better results than either the regression-based polynomial or Weibull curve fit approaches (this is expected as each bin's scale factor is independent of adjacent bins). The greatest differences, as inferred from the max and min profiles in Fig. 8, occur in the upper canopy. This is likely due to simultaneous increases in foliage characterisation with ALS and potentially decreased characterisation by TLS of the uppermost sections of canopy resulting from the differing view geometries and occlusion biases of the respective platforms (Chasmer et al., 2006).

The 3D implementation of the calibrated ALS LAIe model is illustrated in Fig. 9A. A grid resolution of 2 m is used to aid in the visual interpretation of canopy features but the spatial domain of each grid cell is equal to that of the EVI/ALS LAIe calibration radius of 11.3 m or 400 m^2. The bimodal distribution in the canopy foliage is clear with denser vegetation tending to cluster at heights between 3 m to 9 m and 29 m to 35 m. However, while such patterns are also visible in the LAIe profile in Fig. 9B, only the 3D map illustrates the dense clustering of, and large gaps between, foliage elements within the overall canopy space. For example, dense riparian foliage at heights of 2 m to 6 m above the ground surface is visible in Fig. 9A but such vegetation is often more difficult to detect when examining only canopy height models (e.g. Fig. 2). It is not unique to visualise ALS canopy data in this way, as previous studies have also mapped out 3D foliage and gap profiles from ALS data (e.g. Todd et al., 2003). However, this 3D calibration approach builds on earlier attempts by increasing our confidence in the bin-level and cumulative estimates of total LAIe values throughout the canopy.

Comparing the 3D GIS predictions of bin height-level (Fig. 10A) and plot-level total (Fig. 10B) LAIe with those of the EVI training plots illustrates reasonable correspondence, with slopes close to unity and standard errors of 0.03 $m^2\ m^{-2}$ for bin height estimates, and 0.24 $m^2\ m^{-2}$ at the plot-level. In both cases, there is considerable scatter about the best fit line with weak r^2 values. This 'noise' is due to

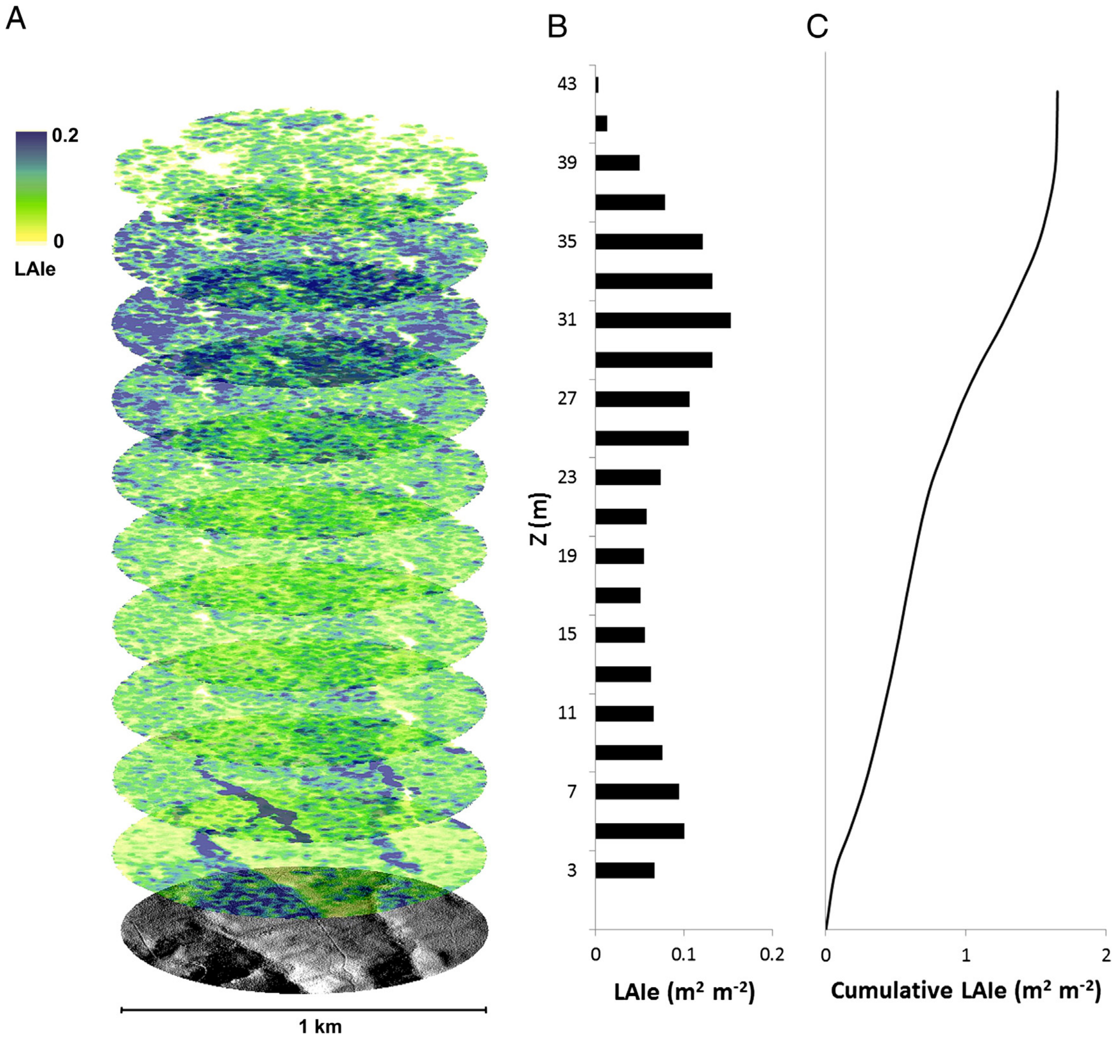

Fig. 9. ALS modelled LAIe for 500 m radius around Tumbarumba flux tower site. A) Profile of spatial distributions of LAIe within every other 2 m height bin from 2 m to 44 m above hillshade ground surface (vertically exaggerated for illustration purposes); B) average LAIe for each 2 m height bin layer surrounding the tower; and C) cumulative LAIe from ground to top of the canopy (max = 1.65 $m^2\ m^{-2}$).

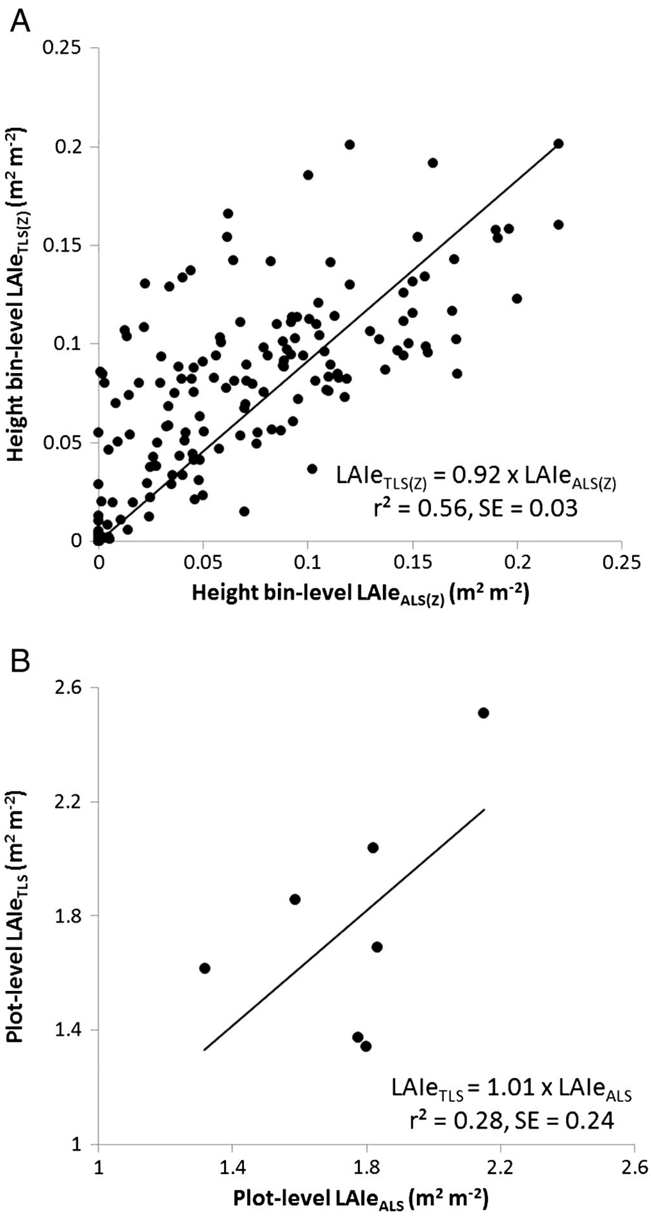

Fig. 10. Calibrated bin height (A) and plot (B) of LAIe after application of the scaling function *a* from Eq. (8).

the inherent spatial variability within the canopy profile at Tumbarumba, and illustrates that no single scaling function can work perfectly across the range of profiles sampled at the seven EVI training plots. Each of the training plots provides a sample of the foliage profile distribution and assuming that the sample plots are representative of the AOI, the calibration derived from the combined training plots is a valid approach.

The average total LAIe for the entire 500 m radius around the Tumbarumba flux tower (Figs. 9C and 11A) is found to be 1.65 $m^2 m^{-2}$ ($\sigma = 0.41$ $m^2 m^{-2}$) whereas the average total LAIe$_{TLS}$ for the seven EVI plots was 1.75 $m^2 m^{-2}$($\sigma = 0.25$ $m^2 m^{-2}$). A t-test demonstrates that there is no significant difference in these estimates, suggesting that the range of profiles sampled at the EVI plots is generally representative of the canopy conditions within the 500 m radius AOI. However, some areas of open canopy and, more importantly, dense riparian understorey foliage that were not sampled in the grid-based EVI training dataset are visible in Figs. 9A and 11A. Due to the grid-based plot set up surrounding the tower and need to capture the full range of canopy height, the EVI training data used here did not sample the complete range of canopy profile conditions throughout the AOI. Consequently, the calibrated scaling function applied to areas of dense riparian foliage is unlikely to be accurate and the true LAIe values are likely to deviate from those predicted. However, the riparian areas in question represent less than 5% of the overall AOI, so the impact to site-level average LAIe will be negligible. To develop a calibration that would adequately represent different land cover classes it would require stratification of the LAIe$_{TLS}$ training and ALS PD data. This is an area of ongoing research.

The simpler ALS return ratio technique from Eq. (2), using an extinction coefficient k of 0.5, results in an average LAIe of 1.19 $m^2 m^{-2}$ (Fig. 11B). Comparing this with the calibrated total LAIe (Fig. 11A) reveals an under-estimation of ~0.5 $m^2 m^{-2}$, which is statistically significant ($p < 0.01$). This suggests that the chosen k value was too high and the assumption of a spherical (random) leaf orientation is inappropriate for the Eucalyptus canopy at Tumbarumba. Accepting the calibrated estimate of total LAIe as truth and using the gap fraction (P) from the return ratio in Eq. (1) and substituting into Eq. (2), produces a k of 0.36. Lower k values than 0.5 indicate more vertically inclined (erectophile) leaf orientation, which is more typical of Eucalyptus canopies (Anderson, 1981). Re-applying $k = 0.36$ to Eq. (2) produces a total LAIe map (Fig. 11C) that displays a similar level of spatial variability ($\sigma = 0.34$ $m^2 m^{-2}$) with the same dominant patterns of high and low density foliage. Acquiring TLS data over large areas is logistically challenging, so a hierarchical approach of calibrating LAIe foliage profiles over relatively small areas (Eqs. 4 to 8), then scaling up to larger areas using the return ratio approach (Eqs. 1 and 2) may be practical if a model of the vertical LAIe profile is not required.

6. Conclusions

The paper has presented a method of calibrating an ALS-based 3D map of forest canopy LAIe from TLS-generated foliage profile data. It was found that a radius of ~11.3 m was appropriate for the integration of ALS data captured from overhead with hemispherical TLS data captured below the canopy. Furthermore, canopy LAIe profiles can be more accurately simulated from all return data than from either primary or secondary returns alone. It should be cautioned, however, that these results are specific to the high density datasets captured at the Tumbarumba Eucalyptus forest site and it is possible that under different data acquisition, canopy height or foliage density conditions, these observations might not hold.

Matching the ALS PD histogram to that of the EVI LAIe$_{TLS}$ profile followed four different approaches. Three based on curve fitting using regression analysis and one using a simple lookup table to identify a histogram scaling function on a height bin by bin basis. In order of overall model fit between the EVI training data and the ALS PD, the lookup table approach was the most accurate with a standard error of 0.01 $m^2 m^{-2}$, the 5th order polynomial scaling function produced a standard error of 0.09 $m^2 m^{-2}$, the double Weibull distribution a standard error of 0.21 $m^2 m^{-2}$, and the single Weibull 0.88 $m^2 m^{-2}$. In the practical implementation at the local scale of the 500 m radius AOI, the lookup table approach was chosen because it provided the most accurate recreation of the scaling factors required to match the ALS PD to the observed foliage profile. This was considered satisfactory, as the priority area for accurate foliage profiles was the area of maximum flux source concentration around the tower and this coincided with the area represented by the EVI plots.

For more widespread application of such a calibration technique, where training sites might be sparsely spaced, or forest canopy is more heterogeneous, it is believed that a regression-based curve fitting approach would be more suitable. This is because a look up table will honour the scale factors on a bin by bin basis even if anomalies are present in the data. A regression-based approach will smooth over such anomalies and provide a more generalised form of the scaling function that should be more widely applicable; i.e. mitigate the influence of anomalies in training data. Therefore, over forested sites containing a range of canopy structural elements and where there is

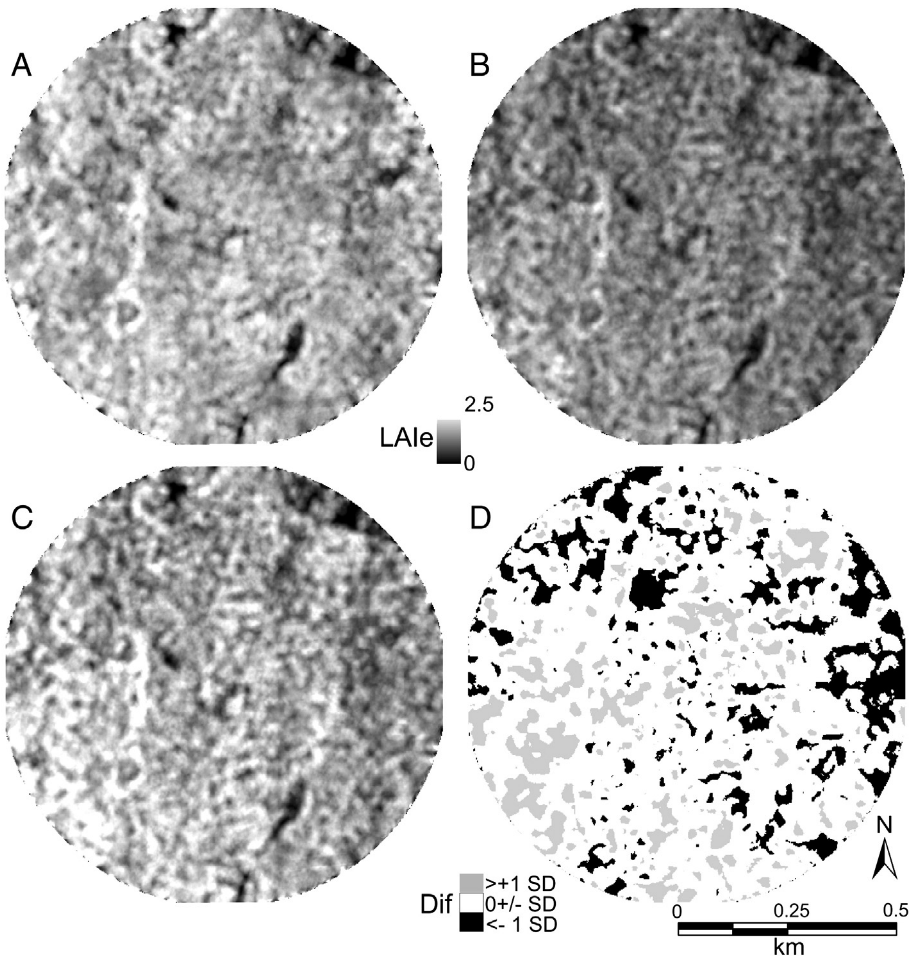

Fig. 11. LAIe maps: A) calibrated total $LAIe_{ALS}$; B) estimated from Eq. (2) using $k = 0.5$; C) estimated from Eq. (2) using optimized $k = 0.36$; and D) difference between A and C (1 standard deviation $= 0.34\ m^2\ m^{-2}$).

confidence that the training plots cover the range of foliage conditions present within the AOI, it might be appropriate to use a polynomial curve to calibrate the scaling function. A single or double Weibull approach is more physically-based, as the shape function has similarities to canopy foliage distributions (Coops et al., 2007; Vose, 1988). Consequently, the use of Weibull scaling functions to match $LAIe_{TLS}$ profiles to ALS PDs would be appropriate for forest stands where the canopy architecture is relatively uniform and/or in situations where training data are very sparse and a more physically-based calibration desired. Regardless of the approach adopted, some sites may contain such canopy heterogeneity or species variety that no single scaling function is appropriate. Under such circumstances, it is recommended that canopy cover be stratified into appropriate classes, and independent scaling functions generated.

While the objective of this study was to derive an accurate 3D map of LAIe at a resolution that could be used as an input to hydrometeorological and carbon flux models at the tree canopy scale, it is clear that this approach can be further adapted and extended. For example, it was shown that the application of a sophisticated foliage profile matching method over a focussed study area can be used to upscale Beer's Law-based estimates of LAIe to larger areas by optimizing the extinction coefficient parameter in Eq. (2). Further, if clumping index and the woody to total foliage ratio are known, it is possible to convert existing estimates of LAIe to true LAI (e.g. Chen et al., 2006; Jonckheere et al., 2005). From Eq. (6) and Lovell et al. (2003, 2012) it is apparent that in addition to the foliage profile, the EVI data can be used to recreate the gap distribution or the variation in transmittance with height in the canopy. A similar histogram-matched scaling function approach to that described could therefore be applied to calibrate an accurate 3D map of canopy transmittance from the inverse of the ALS PD.

Acknowledgements

Jorg Hacker, Aviation Research Australia is acknowledged for collecting and processing the raw ALS data. David Colville and ArantchaCebello are also acknowledged for the assistance in the field. This work was supported by the UK Natural Environment Research Council [NERC] [grant NE/G000360/1], the UK NERC National Centre for Earth Observation (NCEO) [NCEO Mission Support 2009], the UK Royal Society [Grant IE110132] and by grants from the Australian Climate Change Science Program and its predecessors through the DCCEE.

References

Adams, T., Beets, P., & Parrish, C. (2012). Extracting more data from LiDAR in forested areas by analyzing waveform shape. *Remote Sensing*, *4*, 682–702.

Allouis, T., Durrieu, S., Vega, C., & Couteron, P. (2012). Stem volume and above-ground biomass estimation of individual pine trees from LiDAR data: Contribution of full-waveform signals. *ISPRS Journal of Photogrammetry and Remote Sensing*, *99*, 1–11.

Amthor, J. S., Gill, D. S., & Bormann, F. H. (1990). Autumnal leaf conductance and apparent photosynthesis by saplings and sprouts in a recently disturbed northern hardwood forest. *Oecologia*, *84*, 93–98.

Anderson, M. C. (1981). The geometry of leaf distribution in some south-eastern Australian forests. *Agricultural Meteorology*, *25*, 195–205.

Axelsson, P. (1999). Processing of laser scanner data—Algorithms and applications. *ISPRS Journal of Photogrammetry and Remote Sensing*, *54*(No. 2–3), 138–147.

Baltsavias, E. P. (1999). Airborne laser scanning: Basic relations and formulas. *ISPRS Journal of Photogrammetry and Remote Sensing*, *54*(No. 2–3), 199–214.

Blanken, P. D., Black, T. A., Yang, P. C., Neumann, H. H., Nesic, Z., Staebler, R., et al. (1997). Energy balance and canopy conductance of a boreal aspen forest: Partitioning overstory and understory components. *Journal of Geophysical Research*, *102*(No. D24), 28915–28927.

Brümmer, C., Black, T. A., Jassal, R. S., Grant, N. J., Spittlehouse, D. L., Chen, B., et al. (2012). How climate and vegetation type influence evapotranspiration and water use efficiency in Canadian forest, peatland and grassland ecosystems. *Agricultural and Forest Meteorology*, *153*, 14–30.

Chasmer, L., Hopkinson, C., & Treitz, P. (2006). Investigating laser pulse penetration through a conifer canopy by integrating airborne and terrestrial lidar. *Canadian Journal of Remote Sensing*, *32*(2), 116–125.

Chasmer, L., Kljun, N., Barr, A., Black, A., Hopkinson, C., McCaughey, J. H., et al. (2008). Vegetation structural and elevation influences on CO_2 uptake within a mature jack pine forest in Saskatchewan, Canada. *Canadian Journal of Forest Research*, *38*, 2746–2761.

Chen, J. M., Govind, A., Sonnentag, O., Zhang, Y., Barr, A., & Amiro, B. (2006). Leaf area index measurements at FluxNet-Canada forest sites. *Agricultural and Forest Meteorology*, *140*, 257–268.

Chen, J. M., Liu, J., Cihlar, J., & Goulden, M. L. (1999). Daily canopy photosynthesis model through temporal and spatial scaling for remote sensing applications. *Ecological Modelling*, *124*, 99–119.

Coops, N. C., Hilker, T., Wulder, M., St.-Onge, B., Newnham, G., Siggins, A., et al. (2007). Estimating canopy structure of Douglas-fir forest stands from discrete-return LiDAR. *Trees — Structure and Function*, *21*(No. 3), 295–310.

Coops, N. C., Wulder, M. A., & Waring, R. (2012). Modeling lodgepole and jack pine vulnerability to mountain pine beetle expansion into the western Canadian boreal forest. *Forest Ecology and Management*, *274*, 161–171.

Côté, J. -F., Fournier, R. A., & Egli, R. (2011). An architectural model of trees to estimate forest structural attributes using terrestrial LiDAR. *Environmental Modelling and Software*, *26*, 761–777.

Côté, J. -F., Fournier, R. A., Frazer, G. W., & Niemann, K. O. (2012). A fine-scale architectural model of trees to enhance LiDAR-derived measurements of forest canopy structure. *Agricultural and Forest Meteorology*, *166–167*, 72–85.

Davi, H., Bouriaud, O., Dufrêne, E., Soudani, K., Pontailler, J. Y., le Maire, G., et al. (2006). Effect of aggregating spatial parameters on modelling forest carbon and water fluxes. *Agricultural and Forest Meteorology*, *139*, 269–287.

DeWalt, S. J., Maliakal, S. K., & Denslow, J. S. (2003). Changes in vegetation structure and composition along a tropical forest chronosequence: Implications for wildlife. *Forest Ecology and Management*, *182*(No. 1–3), 139–151.

Engel, V. C., Stieglitz, M., Williams, M., & Griffin, K. L. (2002). Forest canopy hydraulic properties and catchment water balance: Observations and modeling. *Ecological Modeling*, *154*, 263–288.

Ge, Z. -M., Zhou, X., Kellomäki, S., Peltola, H., & Wang, K. -Y. (2011). Climate, canopy conductance and leaf area development controls on evapotranspiration in a boreal coniferous forest over a 10-year period: A united model assessment. *Ecological Modelling*, *222*, 1626–1638.

Goetz, S. J., Steinberg, D., Betts, M. G., Holmes, R. T., Doran, P. J., Dubayah, R., et al. (2010). Lidar remote sensing variables predict breeding habitat of a Neotropical migrant bird. *Ecology*, *91*(No. 6), 1569–1576.

Gower, S. T., Kucharik, C. J., & Norman, J. M. (1999). Direct and indirect estimation of leaf area index, fAPAR, and net primary production of terrestrial ecosystems. *Remote Sensing of Environment*, *70*, 29–51.

Holmgren, J., Nilsson, M., & Olsson, H. (2003). Simulating the effects of lidar scanning angle for estimation of mean tree height and canopy closure. *Canadian Journal of Remote Sensing*, *29*(No. 5), 623–632.

Hopkinson, C. (2007). The influence of flying altitude and beam divergence on canopy penetration and laser pulse return distribution characteristics. *Canadian Journal of Remote Sensing*, *33*(No. 4), 312–324.

Hopkinson, C., & Chasmer, L. (2009). Testing LiDAR models of fractional cover across multiple forest ecozones. *Remote Sensing of Environment*, *113*, 275–288.

Hopkinson, C., Chasmer, L., Kljun, N., van Gorsel, E., McCaughey, J. H., Barr, A., et al. (2012). ALS monitoring of changes in above ground forest carbon storage. *In Proceedings of the SilviLaser 2012 Conference, Sept. 16–19, Vancouver, Canada* (Unpaginated USB).

Hopkinson, C., Chasmer, L., Lim, K., Treitz, P., & Creed, I. (2006). Towards a universal lidar canopy height indicator. *Canadian Journal of Remote Sensing*, *32*(No.2), 139–153.

Hopkinson, C., Chasmer, L. E., Young-Pow, C., & Treitz, P. (2004). Assessing plot-level forest metrics with a ground-based scanning lidar. *Canadian Journal of Forest Research*, *34*, 573–583.

Ives, S. L., Sullivan, P. F., Dial, R., Berg, E. E., & Welker, J. M. (2011). CO2 exchange along a hydrologic gradient in the Kenai Lowlands, AK: Feedback implications of wetland drying and vegetation succession. *Ecohydrology*. http://dx.doi.org/10.1002/eco.274.

Jarvis, P. G., & Leverenz, J. W. (1983). Productivity of temperate, deciduous and evergreen forests. In O. L. Lange, P. S. Nobel, C. B. Osmond, & H. Zeigler (Eds.), *Physiological plant ecology IV. Ecosystem processes: Mineral cycling productivity and man's influence. Encyclopedia of plant physiology*, *Vol. 12D*. (pp. 233–280). Berlin: Springer Verlag.

Jonckheere, I., Muys, B., & Coppin, P. (2005). Allometry and evaluation of in situ optical LAI determination in Scots pine: A case study in Belgium. *Tree Physiology*, *25*, 723–732.

Jupp, D. L. B., Culvenor, D. S., Lovell, J. L., & Newnham, G. J. (2005). Evaluation and validation of canopy laser radar (LIDAR) systems for native and plantation forest inventory. *Final Report prepared for the Forest and Wood Products Research and Development Corporation (FWPRDC: PN02.2902)*, CSIRO, Canberra, Australia (Available as CSIRO Marine and Atmospheric Research Paper 020 at http://www.cmar.csiro.au/e-print/open/cmar_rp020.pdf)

Jupp, D. L. B., Culvenor, D. S., Lovell, J. L., Newnham, G. J., Strahler, A. H., & Woodcock, C. E. (2009). Estimating forest LAI profiles and structural parameters using a ground based laser called "Echidna®". *Tree Physiology*, *29*, 171–181.

Kljun, N., Calanca, P., Rotach, M., & Schmid, H. (2004). A simple parameterisation for flux footprint predictions. *Boundary-Layer Meteorology*, *112*, 503–523.

Kljun, N., Rotach, M. W., & Schmid, H. P. (2002). A 3D backward Lagrangian footprint model for a wide range of boundary layer stratifications. *Boundary-Layer Meteorology*, *103*, 205–226.

Kobayashi, H., Baldocchi, D. D., Ryu, Y., Chen, Q., Ma, S., Osuna, J. L., et al. (2012). Modeling energy and carbon fluxes in a heterogeneous oak woodland: A three-dimensional approach. *Agricultural and Forest Meteorology*, *152*, 83–100.

Kowalczyk, E. A., Wang, Y. P., Law, R. M., Davies, H. L., McGregor, J. L., & Abramowitz, G. S. (2006). *The CSIRO Atmosphere Biosphere Land Exchange (CABLE) model for use in climate models and as an offline model.* CSIRO Marine and Atmospheric Research Paper. 013, Aspendale, Victoria: CSIRO Marine and, Atmospheric Research, 1–43.

Leblanc, S. G., Chen, R., Fernandes, R., Deering, D. W., & Conley, A. (2005). Methodology comparison for canopy structure parameters extraction from digital hemispherical photography in boreal forests. *Agricultural and Forest Meteorology*, *129*(No. 3–4), 187–207.

Leuning, R., Cleugh, H. A., Zeglin, S. J., & Hughes, D. (2005). Carbon and water fluxes over a temperate Eucalyptus forest and a tropical wet/dry savanna in Australia: Measurements and comparison with MODIS remote sensing estimates. *Agricultural and Forest Meteorology*, *129*(No. 3–4), 151–173.

Lindberg, E., Olofsson, K., Holmgren, J., & Olsson, H. (2012). Estimation of 3D vegetation structure from waveform and discrete return airborne laser scanning data. *Remote Sensing of Environment*, *118*, 151–161.

Loranty, M. M., Mackay, D. S., Ewers, B. E., Traver, E., & Kruger, E. L. (2010). Competition for light between individual trees lowers reference canopy stomatal conductance: Results from a model. *Journal of Geophysical Research*, *115*, G04019. http://dx.doi.org/10.1029/2010JG001377.

Lovell, J. L., Haverd, V., Jupp, D. L. B., & Newnham, G. J. (2012). The Canopy Semi-analytic PgapAndRadiative Transfer (CanSPART) model: Validation using ground based lidar. *Agricultural and Forest Meteorology*, *158*, 1–12.

Lovell, J. L., Jupp, D. L. B., Culvenor, D. S., & Coops, N. C. (2003). Using airborne and ground-based ranging lidar to measure canopy structure in Australian forests. *Canadian Journal of Remote Sensing*, *29*, 1–16.

Lovell, J. L., Jupp, D. L. B., van Gorsel, E., Jimenez-Berni, J., Hopkinson, C., & Chasmer, L. (2011). Foliage profiles from ground based waveform and discrete point lidar. *Proceedings of the SilviLaser 2011 Conference.Oct. 16–20, Hobart, Tasmania.*

Magnussen, S., & Boudewyn, P. (1998). Derivations of stand heights from airborne laser scanner data with canopy-based quantile estimators. *Canadian Journal of Forest Research*, *28*, 1016–1031.

Magnussen, S., Eggermont, P., & LaRiccia, V. (1999). Recovering tree heights from airborne laser scanner data. *Forest Science*, *45*, 407–422.

Martens, S. N., Ustin, S. L., & Rousseau, R. A. (1993). Estimation of tree canopy leaf area index by gap fraction analysis. *Forest Ecology and Management*, *61*, 91–108.

McAneney, K. J., Brunet, Y., & Itier, B. (1994). Downwind evolution of transpiration by two irrigated crops under conditions of local advection. *Journal of Hydrology*, *161*, 375–388.

Morrison, H., Hopkinson, C., Chasmer, L., & Kljun, N. (2011). Using a GIS approach to optimize effective leaf area index by Canadian boreal forest species using airborne lidar. *Proceedings of the SilviLaser 2011 Conference, Oct. 16–20, Hobart, Tasmania* (Unpaginated USB drive).

Morsdorf, F., Kotz, B., Meier, E., Itten, K. I., & Allgower, B. (2006). Estimation of LAI and fractional cover from small footprint airborne laser scanning data based on gap fraction. *Remote Sensing of Environment*, *104*(No. 1), 50–61.

Næsset, E. (2009). Effects of different sensors, flying altitudes, and pulse repetition frequencies on forest canopy metrics and biophysical stand properties derived from small-footprint airborne laser data. *Remote Sensing of Environment*, *113*(No. 1), 149–159.

Oke, T. R. (1996). *Boundary layer climates.* Routledge: International Thomson Publishing Company, London.

Reitberger, J., Schnörr, C. I., Krzystek, P., & Stilla, U. (2009). 3D segmentation of single trees exploiting full waveform LIDAR data. *ISPRS Journal of Photogrammetry and Remote Sensing*, *64*(No. 6), 561–574.

Riaño, D., Valladares, F., Condes, S., & Chuvieco, E. (2004). Estimation of leaf area index and covered ground from airborne laser scanner (LiDAR) in two contrasting forests. *Agricultural and Forest Meteorology*, *124*(No. 3–4), 269–275.

Richardson, A. D., Anderson, R. S., Arain, M. A., Barr, A. G., Bohrer, G., Chen, G., et al. (2012). Terrestrial biosphere models need better representation of vegetation phenology: Results from the North American Carbon Program Site Synthesis. *Global Change Biology*, *18*, 566–584.

Ross, J. (1981). *The radiative regime and architecture of plant stands.* The Hague: Junk Publishers.

Ryu, Y., Verfaillie, J., Macfarlane, C., Kobayashi, H., Sonnentag, O., Vargas, R., et al. (2012). Continuous observation of tree leaf area index at ecosystem scale using upward-pointing digital cameras. *Remote Sensing of Environment*, *126*, 116–125.

Schwalm, C. R., Williams, C. A., Schaefer, K., Anderson, R., Arain, M. A., Baker, I., et al. (2010). A model-data intercomparison of CO2 exchange across North America: Results from the North American Carbon Program site synthesis. *Journal of Geophysical Research*, *115*, G00H05. http://dx.doi.org/10.1029/2009JG001229, 2010.

Solberg, S., Næsset, E., Hanssen, K. H., & Christiansen, E. (2006). Mapping defoliation during a severe insect attack on Scots pine using airborne laser scanning. *Remote Sensing of Environment*, *102*, 364–376.

Strahler, A. H., Jupp, D. L. B., Woodcock, C. E., Schaaf, C. B., Yao, T., Zhao, F., et al. (2008). Retrieval of forest structural parameters using a ground-based lidar instrument (Echidna). *Canadian Journal of Remote Sensing*, *34*(No. 2), S426–S440.

Todd, K. W., Csillag, F., & Atkinson, P. M. (2003). Three-dimensional mapping of light transmittance and foliage distribution using LiDAR. *Canadian Journal of Remote Sensing*, *29*(No. 5), 544–555.

Traver, E., Ewers, B. E., Mackay, D. S., & Loranty, M. (2010). Tree transpiration varies spatially in response to atmospheric but not edaphic conditions. *Functional Ecology*, *24*, 273–282.

van Gorsel, E., Berni, J., Briggs, P., Cabello-Leblic, A., Chasmer, L., Cleugh, H., et al. (2013). Primary and secondary effects of climate variability on carbon and water exchange in an evergreen Eucalyptus forest. *Agricultural and forest meteorology*. http://dx.doi.org/10.1016/j.agformet.2013.04.27 (In Press).

Vose, J. M. (1988). Patterns of leaf area distribution within crowns of nitrogen- and phosphorus-fertilized loblolly pine trees. *Forest Science*, *34*, 564–573.

Warren-Wilson, J. (1963). Estimation of foliage denseness and foliage angle by inclined point quadrats. *Australian Journal of Botany*, *11*, 95–105.

Watson, D. J. (1947). Comparative physiological studies in growth of field crops. I: Variation in net assimilation rate and leaf area between species and varieties, and within and between years. *Annals of Botany*, *11*, 41–76.

Wedding, J. B., Carlson, R. W., Stukel, J. J., & Bazzaz, F. A. (1975). Aerosol deposition on leaves. *Environmental Science and Technology*, *9*(No. 2), 151–153.

Wehr, A., & Lohr, U. (1999). Airborne laser scanning — An introduction and overview. *ISPRS Journal of Photogrammetry and Remote Sensing*, *54*(No. 2–3), 68–82.

Weiss, M., & Baret, F. (2010). *Can-Eye v6.1 user manual.* French National Institute of Agricultural Research (INRA), 47 (Available online: https://www4.paca.inra.fr/can-eye/Documentation-Publications/Documentation. Last accessed November, 2012)

Weiss, M., Baret, F., Smith, G. J., Jonckheere, I., & Coppin, P. (2004). Review of methods for in situ leaf area index (LAI) determination: Part II. Estimation of LAI, errors and sampling. *Agricultural and Forest Meteorology*, *121*, 37–53.

Whitehead, D., & Kelliher, F. M. (1991). A canopy water balance model for Pinusradiata stand before and after thinning. *Agricultural and Forest Meteorology*, *55*, 109–126.

Wilson, K. B., Hanson, P. J., Mulholland, P. J., Baldocchi, D. D., & Wullschleger, S. D. (2001). A comparison of methods for determining forest evapotranspiration and its components: Sap flow, soil water budget, eddy covariance and catchment water balance. *Agricultural and Forest Meteorology*, *106*, 153–168.

Yang, X., Strahler, A., Schaaf, C., Jupp, D., Yao, T., Zhao, F., et al. (2013). Three-dimensional forest reconstruction and structural parameter retrievals using a terrestrial full-waveform lidar instrument (Echidna®). *Remote Sensing of Environment*, *135*, 36–51.